WILEY-VCH

DOI: 10.1002/ ((please add manuscript number))
Article type: Full Paper

Band bending engineering at organic/inorganic interfaces using organic self-assembled monolayers

Oliver T. Hofmann and Patrick Rinke*

Dr. Oliver T. Hofmann
Graz University of Technology, Institute of Solid State Physics, NAWI Graz
Petersgasse 16/II, 8010 Graz, Austria
o.hofmann@tugraz.at

Prof. Patrick Rinke
COMP/Department of Applied Physics,
Aalto University, P.O. Box 11100, Aalto FI-00076, Finland

Keywords: oxide interfaces, electrode/molecule contacts, theory & simulation, surface modification and engineering, organic/inorganic interfaces

Abstract

Adsorbing strong electron donors or acceptors on semiconducting surfaces induces band bending, whose extend and magnitude are strongly dependent on the doping concentration of the semiconductor. Here we apply hybrid density-functional theory calculations together with the recently developed charge reservoir electrostatic sheet technique (CREST) (Sinai et al, PRB, 91 (7) 075311, 2015) to account for charge transfer from the bulk of the semiconductor to the interface. We then investigate the impact of surface-functionalization with specifically tailored self-assembled monolayers (SAMs). For the example of three chemically very similar SAMs, that all bond to the ZnO surface via pyridine docking groups, we show that the SAMs introduce shallow or deep donor levels that pin the band bending at the position of the SAM's highest occupied molecular orbital. In this way, the magnitude of the induced band bending can be controlled by the type of SAM, to a point where the doping-concentration dependence is completely eliminated.

1. Introduction

Organic photovoltaic cells and light-emitting devices require at least one transparent electrode such that light can reach or leave the organic material in which it is produced from or converted to electricity. Although in principle such electrodes can be realized using nano-scale metals, it is more convenient to use doped, large band-gap transparent conductive oxides, such as ZnO. Often, these optically active organic materials are not in direct contact with ZnO. Instead, molecular electron acceptors are sandwiched between the optical organic material and ZnO, either because the electron acceptors are part of the active organic materials (e.g. fullerenes in photovoltaic cells[1–4]) or to modify the work function of ZnO, and therefore the charge injection and extraction barriers (as in the case of, e.g., CuPc[5], PTCDA[5,6], or F4TCNQ[7]).

The electron acceptors receive charge from the semiconductor until their acceptor levels are energetically in resonance with the Fermi energy. The resulting ground-state charge transfer across the interface gives rise to the formation of a space-charge region and associated band bending. This space-charge region can affect the charge-transport properties across the interface and significantly weakens the binding between substrate and adsorbate.[8] The spatial extent and the magnitude of the band bending depend on the amount of charge-transfer from the bulk to the adsorbate as well as on the bulk doping concentration and profile. Experimentally, those parameters are often challenging to control and not always well known. Moreover, they are subject to change during device operation, e.g. due to migration of charged defects, impeding the long-term stability of (opto)electronic devices.

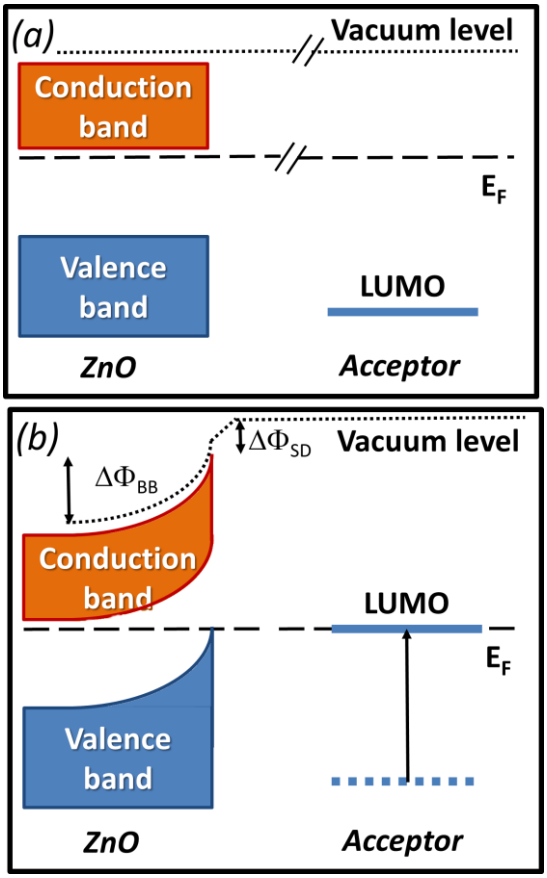

Figure 1: Schematic level alignment at a semiconductor/organic interface (a) prior and (b) upon interaction. $\Delta\Phi_{BB}$ denotes the change in the electrostatic potential due to band bending, $\Delta\Phi_{SD}$ is the surface dipole.

When the electron affinity of the adsorbate is larger than the substrate's work function, i.e. when the lowest unoccupied molecular orbital (LUMO) is below the Fermi-energy (E_F) as schematically shown in **Figure 1a**, the bulk crystal donates electrons to the adsorbate. The ensuing dipole moment ($\Delta\Phi$) shifts the now partially occupied LUMO upwards in energy until it is in resonance with the Fermi-energy[9,10].

The overall interface dipole $\Delta\Phi$, is often divided into a band bending contribution $\Delta\Phi_{BB}$ (i.e. the long-range, quasi-parabolic potential within the substrate), and a surface-dipole contribution $\Delta\Phi_{SD}$ (the approximately linear potential change in the "empty" space between substrate and adsorbate), as indicated in Figure 1b. The relative contribution of $\Delta\Phi_{BB}$ and $\Delta\Phi_{SD}$ depends strongly on the doping concentration of the substrate[8]. In principle, for low doping concentrations and strong electron acceptors, band bending could be as large as the

total band gap of the substrate (ca. 3.5eV in ZnO). In practice, however, $\Delta\Phi_{BB}$ is almost always limited by the presence of defect states at or near the surface, such as oxygen vacancies,[11–13] provided they are present in sufficient concentrations.

Since the type and concentration of these defects is difficult to control, band bending is typically hard to engineer. In this article, we use these defect states as an analogy to demonstrate a new concept that uses properly designed, covalently attached self-assembled monolayers (SAMs) to act like surface defects that limit band bending at desired values. In order to do so, the highest occupied molecular orbitals (HOMOs) of theses SAMs need to lie within the band gap of the inorganic substrate. This situation is schematically shown in Figure 2. Upon contact with the organic adsorbate, band bending will emerge until it shifts the SAM-HOMO up to the Fermi-energy. As soon as the SAM-HOMO becomes resonant with the Fermi energy, charge transfer from the SAM towards the adsorbate opens up as additional electron-transfer channel, thereby inhibiting any further band bending. The SAM thus acts akin to deep donor states. While conventional deep donor states are usually intrinsic to a material and thus found at fixed energies, using organic SAMs opens up the vast toolbox of organic chemistry to us. It is possible to design SAMs with states at desired energies and thereby control the energy landscape and the exact amount of band bending at the interface. With this design principle it is possible to create organic electronic devices that are less dependent on the growth conditions of the semiconductor substrate (and, hence, its doping concentration) and that exhibit a better long-term stability.

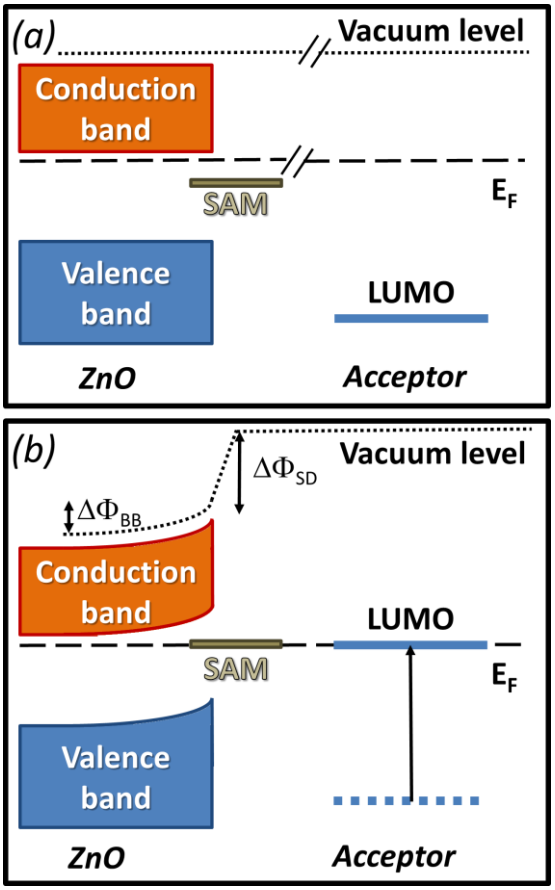

Figure 2: Schematic level alignment at a semiconductor/SAM/organic interface (a) prior and (b) upon interaction. $\Delta\Phi_{BB}$ denotes the change in the electrostatic potential due to band bending, $\Delta\Phi_{SD}$ is the surface dipole.

To demonstrate this concept, we study the interface between a SAM-functionalized ZnO(1 0 $\overline{1}$ 0) surface and a tetracyano-quinodimethane (**TCNQ**) layer. TCNQ is a typical, strong electron acceptor that is frequently used for level-alignment studies, in particular in conjunction with other organic materials.[14–22] To functionalize the interface between ZnO and TCNQ, we consider three organic SAMs: doubly reduced viologen (**Vio**), diamino-4-phenyl-pyridine (**DAPP**), and 2,5- *para*-phenylpyridine (**PPP**). The molecules, whose chemical structures are shown in Figure 3, are listed here in order of their *increasing* ionization potential (*decreasing* HOMO, *vide infra*). In all molecules we used pyridine as docking group, which has been shown to form stable (2x2) patterns on ZnO(1 0 $\overline{1}$ 0) without inducing appreciable etching.[23–25] Moreover, a full monolayer of pyridine reduces the work function of

ZnO(10-10) by almost 3.0 eV[25] and therefore increases the charge-transfer across the interface, amplifying the effect that we intend to show here. It is worthwhile mentioning here that the introduction of these polar layers does not affect the final work function upon TCNQ deposition,[26] changes in the geometric structure notwithstanding. For the sake of demonstrating the concept, we consider atomistically clean, defect-free ZnO. Accounting for additional deep donor states,as done e.g. in ref 6, is straightforward but would unduly complicate the calculations and the interpretation of the results.

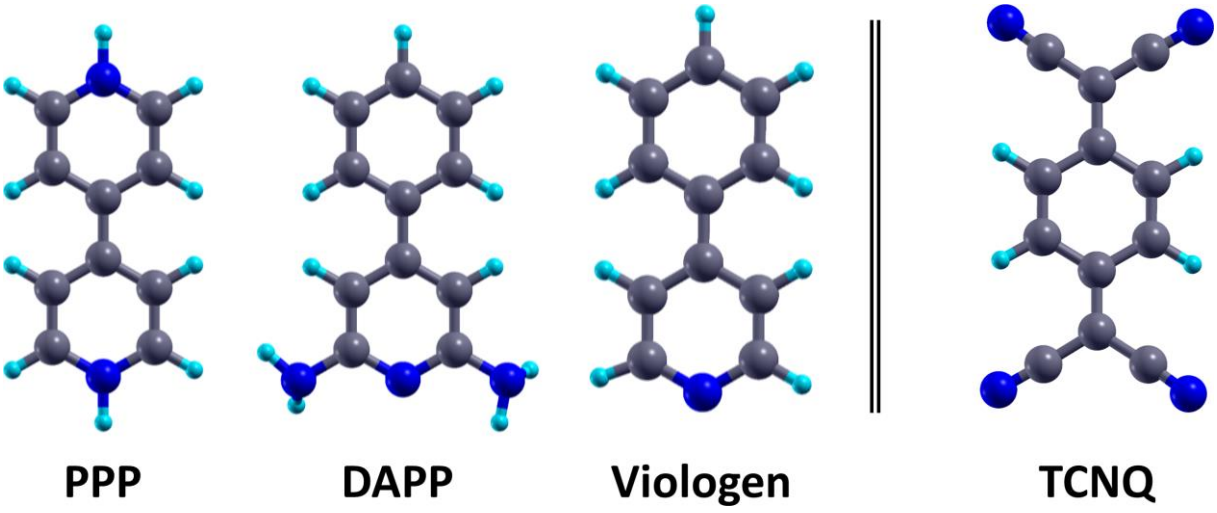

Figure 3: Chemical structure of the molecules used in this work: para-phenylenepyridine (PPP), 2,5-diamino para-phenylenepyridine (DAPP), and Viologen (Vio) serve as surface functionalization. Tetracyanoquinodimethane (TCNQ) is the electron acceptor. Grey balls denote carbon atoms, blue nitrogen atoms, and cyan balls correspond to hydrogen.

All studies were performed using density functional theory in the repeated-slab approach, employing the HSE06 hybrid functional family.[27,28] We increase the fraction of exact exchange to 40% to improve the description of the band gaps as well as the valence band width of ZnO (as demonstrated in references 29,30,25). We have previously reported that the choice of the functional does not affect the interface dipole generated by the adsorption of pyridine-SAMs.[25] To account for long range van-der-Waals interactions, we used the vdW-TS[31] scheme with the appropriate parameterization for metal oxides.[32] Band bending and doping is treated using a simplified version of the Charge Reservoir Electrostatic Sheet Technique (CREST).[33,34] In short, CREST simulates the space-charge region by a negatively

charged sheet placed on the backside of the slab. The charge and position of the sheet is determined self-consistently, using only the substrates doping concentration N_D and its dielectric constant as parameters. Within the quantum-mechanically treated ZnO slab, we accounted for the variable n-type doping by means of the virtual crystal approximation (VCA).[35] More details are given in the Method Section at the end of this paper.

2. Results and discussion

2.1. TCNQ on non-functionalized ZnO

To establish a reference, a useful first step is to examine the adsorption of TCNQ on the pristine, unaltered ZnO surface. We consider two morphologies: (1) a low-density structure in which TCNQ molecules are adsorbed face-on (i.e. flat lying), and (2) a high-density structure in which TCNQ molecules adsorb edge on (i.e. upright standing). Our calculations show that TCNQ can assume several adsorption geometries on ZnO(10-10) that are energetically very close to each other. Hence, we would expect that in experiments, TCNQ would probably form disordered films. Since a full structure search or an investigation of disordered films is beyond the scope of the present paper, the two ordered morphologies can be regarded as "extreme cases" of different adsorption structures. Hereafter, we will focus on the upright standing TCNQ film, shown as inset in Figure 4, since TCNQ also assumes a similar adsorption geometry upon adsorption on the self-assembled monolayers (see below). It should be emphasized, however, that the doping dependence of the adsorption induced band bending agree qualitatively for the flat-lying and the upright-standing geometry.

The band-banding contribution to the adsorption-induced work function change is shown as a function of the ZnO doping concentration in Figure 4. We chose to define band bending by the *change* of the onset of the ZnO valence band (with respect to the Fermi-energy) of the ZnO/SAM/TCNQ system relative to the pristine ZnO surface. We find that the work function after adsorption is essentially independent of the bulk doping concentration (ca. 6 eV), as

previously observed for F4TCNQ on the polar ZnO surface.[7,8] At the lowest considered doping concentration (N_D = 10^{16} e/cm³), the band bending is $\Delta\Phi^{BB}$ = 3.1 eV and thus of the same order of magnitude as the band gap. For larger doping concentrations, $\Delta\Phi^{BB}$ becomes smaller. The change of $\Delta\Phi^{BB}$ with N_D is relatively small between 10^{16} e/cm³ and 10^{18} e/cm³. For larger N_D, however, $\Delta\Phi^{BB}$ decreases exponentially, until it vanishes for degenerately doped ZnO (N_D = 10^{21} e/cm³). Natively doped ZnO is expected to contain 10^{17} e/cm³ or more.[36] The large sensitivity of $\Delta\Phi^{BB}$ to N_D at this value further illustrates the importance of controlling the band bending through surface functionalization.

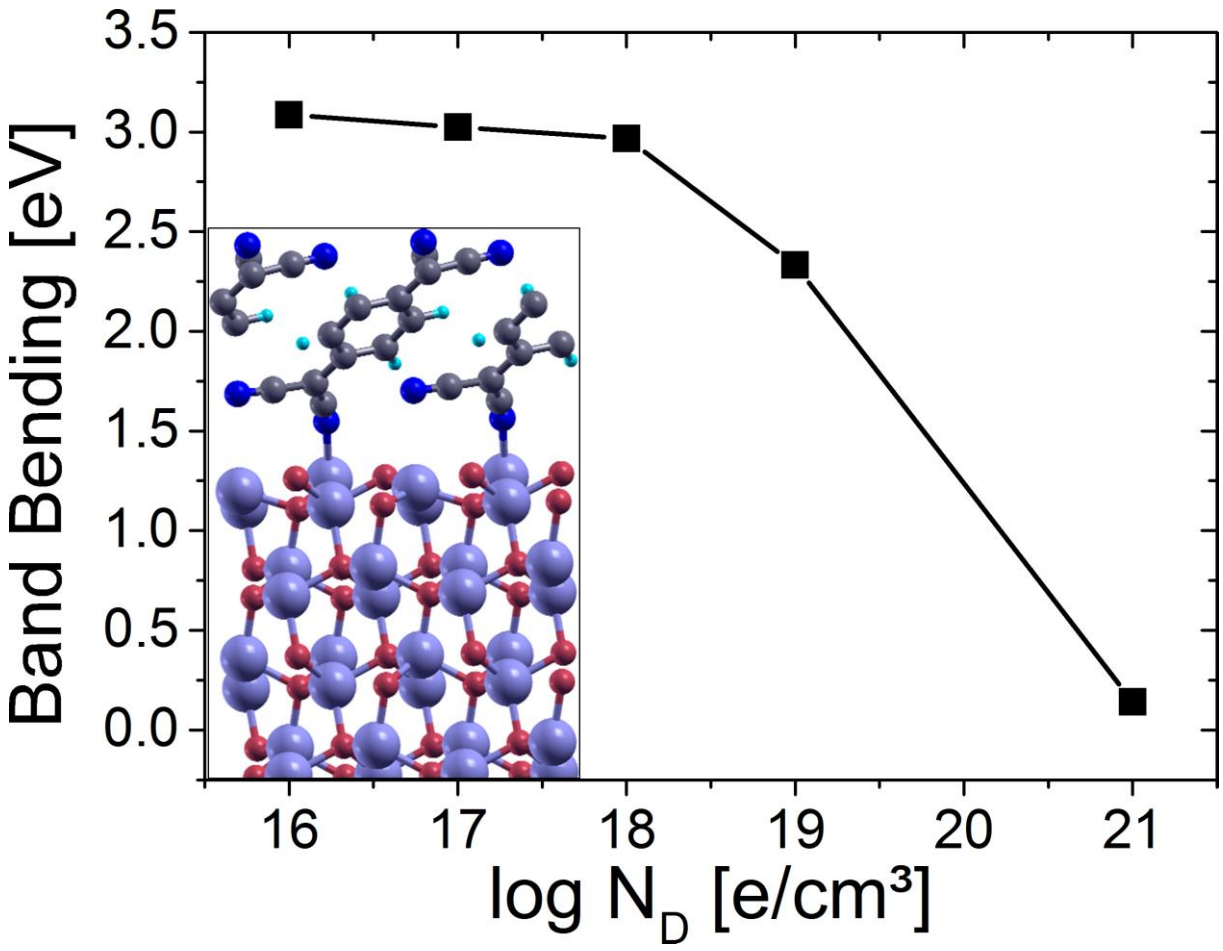

Figure 4: Adsorption-induced band bending as function of the substrate doping concentration for an upright-standing TCNQ film on the ZnO(10-10) surface.

2.2. Surface functionalization of ZnO

To demonstrate the impact of specifically customized self-assembled monolayers on the level alignment between TCNQ and ZnO, we consider three different archetypes, which are characterized by the position of the molecular HOMO with respect to the ZnO band gap.

2,5-*para*-phenylpyridine (**PPP**) serves as our "blind-test". Its ionization energy is sufficiently large that its DFT HOMO lies below the valence band maximum (VBM) of ZnO, and its gap is large enough such that its LUMO is located above the conduction band minimum (CBM) of ZnO. In other words, PPP does not induce states in the ZnO band gap, as shown in Figure 5. The second molecule in our study is diamino-4-phenyl-pyridine (**DAPP**). Although this molecule is chemically very similar to PPP, the two amine groups and their corresponding dipole moments decrease the ionization potential of DAPP significantly. On the surface, the HOMO of DAPP is found in the ZnO gap, approx. 2.3 eV below the Fermi energy (E_F). Finally, Viologen (**Vio)** is a particular strong electron donor[37–40] due to its quinoid structure. It exhibits a HOMO 0.1 eV below the conduction band edge and thus directly at the Fermi energy.

Our calculations indicate that all three SAMs adopt a similar morphology on the surface, as shown in the SI. In analogy to the interaction of unsubstituted pyridine with ZnO(10-10),[23–25] all molecules adsorb with the nitrogen lone pair situated above a surface Zn atom. The energetically most stable packing density (at 0 K and omitting the zero-point energy) is found at 5.8 molecules / nm², which amounts to one molecule being bonded to every second surface Zn atom. A tighter molecular packing is less stable due to steric repulsion between the molecules in the layer.

In experiments, ZnO is typically n-type doped,[41] with its Fermi level ca. 200 meV below the conduction band onset. Since all SAMs considered here are electrons donors, they potentially introduce downward band bending, which is limited by the difference between the conduction

band and E_F. We have recently verified for pyridine that our surface slab models contain enough ZnO layers to capture this downward band bending.[25] The interface dipole induced by the adsorption of the SAMs causes a strong reduction of the work function of the substrate from 4.6 eV (pristine) to 1.2 eV (Vio), 2.9 eV (DAPP), and 1.7 eV (PPP). (Note that the work-function modification induced by the SAMs does not correlate with the ionization potential because of the molecules' inherent dipole moment.) Intuitively, one might assume that the different work function of the ZnO/SAM system will impact the level alignment of subsequently deposited TCNQ. However, for molecules which are in the so-called Fermi-level pinning region (i.e., where a molecular state is in resonance with the Fermi-energy after adsorption), we have previously shown that any dipole that is spatially located between the charge reservoir (here: ZnO) and the adsorbate (TCNQ) has no net effect on the final work function;[26] a claim that, as will be shown in the following, is corroborated by the observation that the work-function after TCNQ deposition is essentially independent of the underlying SAM.

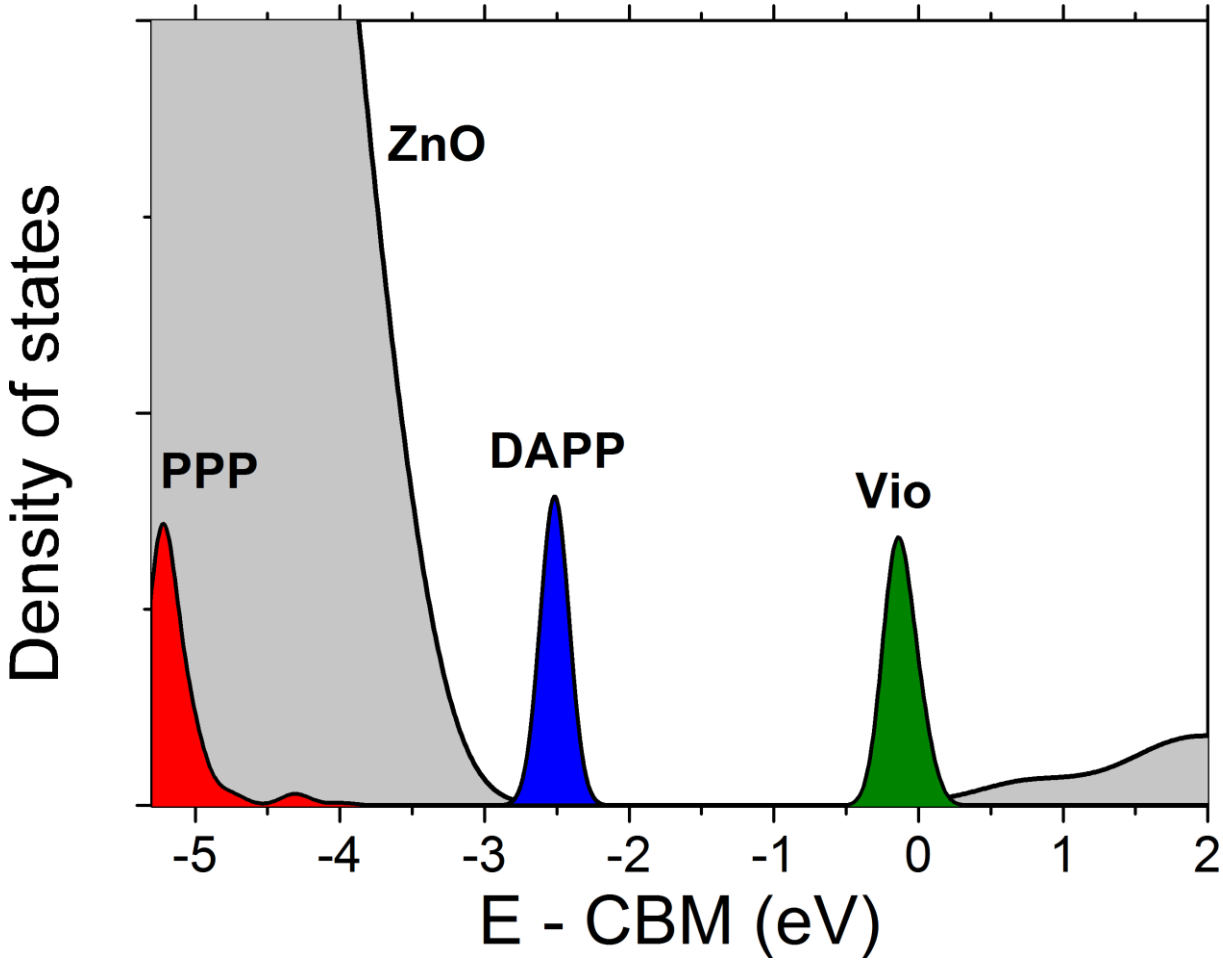

Figure 5: Level alignment between ZnO(10-10) and the three SAMs PPP (red), DAPP (blue), and Vio (green). For the sake of clarity, only the HOMO of the SAMs is shown. A density of states with all molecular contributions can be found in the SI.

2.3 Adsorption of TCNQ on functionalized ZnO

On all three SAMs, we find that TCNQ adopts a roughly upright-standing geometry, shown in the Supporting Information. If there would be no interaction between the TCNQ film and the ZnO/SAM system, the TCNQ LUMO would be located 6.2 - 6.5 eV below the vacuum level in our calculations. The difference occurs due to the slightly different inclination of the TCNQ molecules with respect to the surface normal.[42] Under the assumption of vacuum level alignment (i.e., the non-interacting limit), ε_{LUMO} is thus sufficiently low to be located below the HOMO of **Vio** and **DAPP**, but not of **PPP**. Furthermore, it is always below the conduction band onset of ZnO. Therefore, electron transfer from the inorganic substrate to TCNQ should be expected in all three cases.

To understand the processes occurring upon adsorption of TCNQ on the SAM/ZnO surfaces, it is instructive to first consider the "metallic limit". "Metallic limit" here refers to a situation in which the substrate is so strongly doped such that the bands are practically flat and the little bit of (upward) band bending induced by electron transfer from "bulk" ZnO to its surface is confined to a few Å. In other words, all band bending is completely captured in a slab calculation with only 8 ZnO layers. Here we used a doping concentration of 10^{21} e/cm^3 to achieve this metallic limit. The resulting level alignment, shown in Figure **6a-c,** shows that (i) that there is no appreciable band bending, illustrated by the observation the conduction band edge of the topmost layers is still below the Fermi energy, and (ii) that the TCNQ LUMO shifts into resonance with the Fermi-energy in all three cases. Consequently, we observe a fractional filling of the (former) TCNQ LUMO upon adsorption.[1] A Mulliken charge analysis shows that each TCNQ molecule accepts approx. 0.60 e on **Vio**, 0.13 e on **DAPP**, and 0.15 e on **PPP**.

[1] We note that since there is no wave-function overlap between ZnO and the TCNQ molecules, no hybrid states form. In previous work, we showed that in such cases integer charge transfer would be expected[43]. The fact that we observe partial and not integer charge transfer in our calculations in this work is partly a result of the self-interaction error still present in the hybrid functional we use[43–45] the small lateral size of the unit cell that does not permit charge localization of individual molecules. The distinction between integer and fractional charge transfer does not affect our results here. Nonetheless, the partial filling in our calculations should be interpreted as ensemble-average of charged and neutral TCNQ molecules, in the same sense as the virtual crystal approximation representing an ensemble average of substrate and dopant atoms.

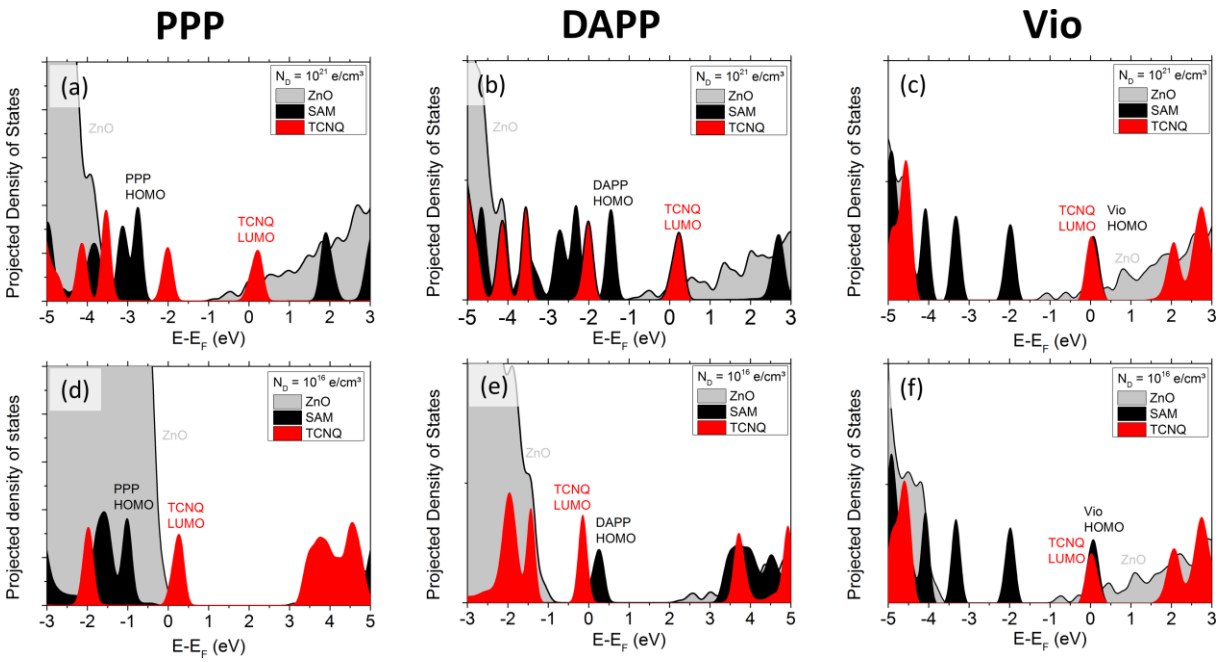

Figure 6: Level alignment for TCNQ on modified ZnO. Panels a-c show the level alignment upon contact with the TCNQ crystal for metallic doping. Panels d-f show the level alignment upon contact for a doping concentration of 10^{16} e/cm³. For ZnO only the projection onto the four topmost double layers is shown.

The combined systems exhibit total work functions of 6.3-6.8eV, agreeing well with the LUMO-energy of the non-interacting monolayer. We emphasize again that because the SAM is located between the charge reservoir (ZnO) and the pinned system (TCNQ), its dipole moment has essentially no impact at all on the final work-function of the pinned system.[26] The interface dipole also shifts the states of the SAM significantly upward in energy. For **Vio**, the HOMO is now in resonance with the TCNQ LUMO. This shows that **Vio** directly donates charge to TCNQ and explains why the LUMO occupation is so much higher than for the other two SAMs. **DAPP** shows an increase of the HOMO energy from 2.3 eV to 1.3 eV below E_F, with the HOMO still being significantly beneath the TCNQ LUMO. Also **PPP** shows a significant increase of its HOMO energy, which is now found in the ZnO gap, but still far below the TCNQ LUMO (see Figure 6).

As next step, we consider more realistic doping concentrations. In particular for low doping concentrations, the spatial extend of the depletion region can reach macroscopic dimensions. In general, it is not possible to model slabs which are sufficiently large to capture the whole region. We therefore employ the CREST method.[33]

In **Figure 6d-f**, the level alignment for all three systems is shown exemplarily for a doping concentration of 10^{16} e/cm³. The ZnO/Vio/TCNQ system does not exhibit any band bending, since the HOMO of Vio lies directly at the Fermi-energy already prior to adsorption and hence, does not require any band bending to induce charge-transfer from the SAM to the adsorbate. For Zno/DAPP, the HOMO was initially 2.4 eV below the Fermi-energy. DAPP is thus only able to contribute to the chargetransfer to TCNQ once its HOMO has been shifted to the Fermi-energy by virtue of band bending, i.e. at a band bending value that corresponds to the difference of the HOMO to the Fermi-energy prior to interaction. Indeed, upon TCNQ adsorption, we calculate a band bending of approx. 2.4 eV. Consequently, now the DAPP-HOMO is found in resonance with the Fermi energy and pins it. We emphasize here once again that our model for the ZnO slab does not include other deep donor states except for those induced by the SAM. In reality, it is likely that such states would be present and pin the band bending already at a smaller value. Nonetheless, the results nicely corroborate the fundamental mechanism proposed in Figure 2. Conversely, for the Zno/PPP system the SAM-HOMO is below the VBM of ZnO. Once band bending has developed, the valence band reaches the Fermi-energy before the PPP-HOMO does, and hence the band bending is only limited by the magnitude of the ZnO band gap.

To ascertain the stability of the result, we have calculated the level alignment for doping concentrations between 10^{16} e/cm³ and 10^{19} e/cm³. The result for the band bending is depicted in Figure 7. Within the calculated doping range, there is no band bending for ZnO/Vio. For ZnO/DAPP, the band bending is mostly constant between 10^{16}-10^{18} e/cm³, and slightly decreases at higher doping concentration. For PPP, the band bending always amounts to the maximum possible value, i.e. 3.5 eV, corresponding to the ZnO band gap in our calculations. These three molecules are therefore examples of the three different possible types of band bending achievable in these ternary systems: constant band bending at minimum and

maximum value and band bending pinning at a predesigned value with a small residual doping dependence for higher doping concentrations.

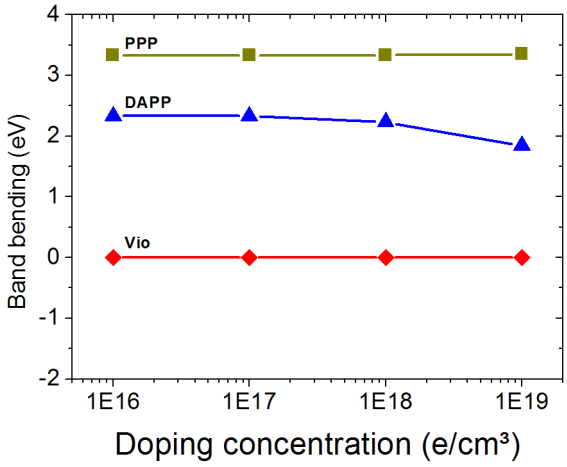

Figure 7: Band bending after TCNQ adsorption on ZnO/SAM, as function of the ZnO doping concentration

In summary, we have shown that self-assembled monolayers can limit band bending at interfaces between inorganic electrodes and organic electronic acceptors. The maximum amount of band bending can be tuned by tuning the HOMO energy of the employed SAM. Particularly strong electron acceptors, such as Viologen, are even able to suppress band bending completely. SAMs with a HOMO in the gap pin the band bending at a predetermined energy, akin to deep donor states. Conversely, adsorbates with their HOMO below the valence-band maximum, do not have any impact on the magnitude of the band bending.

Our results indicate that the toolbox of organic chemistry can be used to design surface-modifications, which generally mitigate or even completely suppress the occurrence of band bending in transparent conductive oxides. We expect that the application of such molecules makes the performance of organic electronic devices less dependent on unintentional doping during the crystal growth process or to changes of the doping concentration during device operations. Such devices may exhibit a better device performance and a better long-term stability.

Method Section

Calculations were performed using the FHI-aims code[46,47] with a numerically tabulated atomic orbital basis. Surfaces and interfaces were modelled by periodic slabs containing four double-layers of ZnO. A Gamma-centered k-grid of 16x16x1 points per ZnO unit cell has been used and scaled appropriately to larger supercells. A region of at least 30 Å vacuum was inserted between the slab and its periodic replica. In the direction perpendicular to the surface, dipole interactions between repeated slabs were prevented by using a dipole correction.[48] We used FHI-aims' "tight" numerical, which also implies a "Tier 1" basis for Zn and a "Tier 2" basis for all other atoms. The electronic structure was calculated using the HSE06 functional[27,28] with 40% instead of the usual 25% exact exchange. The same amount of exact exchange was used in previous studies[8,30], and similar values (37.5%) have been used by others.[29,49] All geometry optimizations were performed using the Perdew, Becke and Ernzerhof (PBE) [50] generalized gradient approximation corresponding to HSE with 0% exact exchange. To account for long-range van-der-Waals forces, we employed the vdW-TS scheme.[31] For ZnO, the parameters were obtained from time-dependent density functional theory.[32] We used C_6 = 46.0183, α = 13.7743, r_0 = 2.818 for Zn and C_6 = 4.45343, α = 4.28501, r_0 = 2.953 for O, as previously published in Reference. [25] The SCF-cycle was converged to a threshold of 10^{-6} eV for the total energy and 10^{-3} eV for the sum of eigenvalues. All geometries were optimized using the PBE+vdW functional until the remaining forces were smaller than 10^{-3} eVÅ^{-1}.

Due to its low-lying valence band, bulk ZnO is always found to be n-type doped.[51] In the present work, we use a modified version of the CREST method to account for doping.[33,34] CREST treats a part of the substrate (the surface) within DFT, while the long-range electrostatic behavior (i.e., in particular the band bending) is captured semi-classically using a charged plate at the bottom of the slab. Within the quantum-mechanically treated substrate,

we employ the virtual crystal approximation to model the free charge carriers.[30,52,53] Here, the oxygen atoms are replaced using an electrically neutral pseudo-atom that contains a core with a charge of 8+δ and the same number of electrons. The excess electrons go to the bottom of the conduction band.

Any band bending beyond the slab is modelled quasi-classical by using a charged plate. In short, the charge of the plate is computed by requiring that adsorbing a molecule on the upper side of the slab must not change the position of the Fermi-level (i.e., the work function) on the bottom side of the slab. The position of the charged plate is then determined from the overall charge and the doping concentration. A more comprehensive explanation will be given in a future publication. In contrast to the original formulation, the simplified version of CREST used in this paper requires only the dielectric constant ε of ZnO and the work-function of the unperturbed slab as input. We used ε =4 for ZnO. The work-function of the unperturbed slab was determined from a separate calculation without the adsorbate for each doping concentration separately. The CREST-approach works self-consistently and was converged to an accuracy of the work function of 100 meV.

Supporting Information

Supporting Information is available online from the Wiley Online Library or from the author.

Acknowledgements

Funding by the FWF-projects J-3258 and P27868 and the collaborative research center (SFB) 951 of the German Science Foundation is gratefully acknowledged. This work was supported by the Academy of Finland through its Centres of Excellence Programme under Projects No. 251748 and No. 284621. The computational results presented have been achieved in part using the Vienna Scientific Cluster (VSC). This research used resources of the Argonne

Leadership Computing Facility, which is a DOE Office of Science User Facility supported under Contract DE-AC02-06CH11357.

(1) White, M. S.; Olson, D. C.; Shaheen, S. E.; Kopidakis, N.; Ginley, D. S. Inverted Bulk-Heterojunction Organic Photovoltaic Device Using a Solution-Derived ZnO Underlayer. *Appl. Phys. Lett.* **2006**, *89*, 143517.
(2) Takanezawa, K.; Hirota, K.; Wei, Q.-S.; Tajima, K.; Hashimoto, K. Efficient Charge Collection with ZnO Nanorod Array in Hybrid Photovoltaic Devices. *J. Phys. Chem. C* **2007**, *111*, 7218–7223.
(3) Hsieh, C.-H.; Cheng, Y.-J.; Li, P.-J.; Chen, C.-H.; Dubosc, M.; Liang, R.-M.; Hsu, C.-S. Highly Efficient and Stable Inverted Polymer Solar Cells Integrated with a Cross-Linked Fullerene Material as an Interlayer. *J. Am. Chem. Soc.* **2010**, *132*, 4887–4893.
(4) Hau, S. K.; Yip, H.-L.; Ma, H.; Jen, A. K.-Y. High Performance Ambient Processed Inverted Polymer Solar Cells through Interfacial Modification with a Fullerene Self-Assembled Monolayer. *Appl. Phys. Lett.* **2008**, *93*, 233304.
(5) Komolov, A. S.; Møller, P. J.; Mortensen, J.; Komolov, S. A.; Lazneva, E. F. Electronic Properties of a Zinc Oxide Surface Modified by Ultra-Thin Layers of Conjugated Organic Molecules. *Surf. Sci.* **2005**, *586*, 129–136.
(6) Gruenewald, M.; Schirra, L. K.; Winget, P.; Kozlik, M.; Ndione, P. F.; Sigdel, A. K.; Berry, J. J.; Forker, R.; Brédas, J.-L.; Fritz, T.; *et al.* Integer Charge Transfer and Hybridization at an Organic Semiconductor/Conductive Oxide Interface. *J. Phys. Chem. C* **2015**, *119*, 4865–4873.
(7) Schlesinger, R.; Xu, Y.; Hofmann, O. T.; Winkler, S.; Frisch, J.; Niederhausen, J.; Vollmer, A.; Blumstengel, S.; Henneberger, F.; Rinke, P.; *et al.* Controlling the Work Function of ZnO and the Energy-Level Alignment at the Interface to Organic Semiconductors with a Molecular Electron Acceptor. *Phys. Rev. B* **2013**, *87*.
(8) Xu, Y.; Hofmann, O. T.; Schlesinger, R.; Winkler, S.; Frisch, J.; Niederhausen, J.; Vollmer, A.; Blumstengel, S.; Henneberger, F.; Koch, N.; *et al.* Space-Charge Transfer in Hybrid Inorganic-Organic Systems. *Phys. Rev. Lett.* **2013**, *111*.
(9) Braun, S.; Salaneck, W. R.; Fahlman, M. Energy-Level Alignment at Organic/Metal and Organic/Organic Interfaces. *Adv. Mater.* **2009**, *21*, 1450–1472.
(10) Hofmann, O. T.; Atalla, V.; Moll, N.; Rinke, P.; Scheffler, M. Interface Dipoles of Organic Molecules on Ag(111) in Hybrid Density-Functional Theory. *New J. Phys.* **2013**, *15*, 123028.
(11) Dulub, O.; Boatner, L. A.; Diebold, U. STM Study of the Geometric and Electronic Structure of ZnO(0001)-Zn, (0001)-O, (1010), and (1120) Surfaces. *Surf. Sci.* **2002**, *519*, 201–217.
(12) Li, H.; Schirra, L. K.; Shim, J.; Cheun, H.; Kippelen, B.; Monti, O. L. A.; Bredas, J.-L. Zinc Oxide as a Model Transparent Conducting Oxide: A Theoretical and Experimental Study of the Impact of Hydroxylation, Vacancies, Interstitials, and Extrinsic Doping on the Electronic Properties of the Polar ZnO (0002) Surface. *Chem. Mater.* **2012**, *24*, 3044–3055.
(13) Kelly, L. L.; Racke, D. A.; Schulz, P.; Li, H.; Winget, P.; Kim, H.; Ndione, P.; Sigdel, A. K.; Brédas, J.-L.; Berry, J. J.; *et al.* Spectroscopy and Control of near-Surface Defects in Conductive Thin Film ZnO. *J. Phys. Condens. Matter* **2016**, *28*, 94007.
(14) Ishii, H.; Sugiyama, K.; Yoshimura, D.; Ito, E.; Ouchi, Y.; Seki, K. Energy-Level Alignment at Model Interfaces of Organic Electroluminescent Devices Studied by UV Photoemission: Trend in the Deviation from the Traditional Way of Estimating the Interfacial Electronic Structures. *IEEE J. Sel. Top. Quantum Electron.* **1998**, *4*, 24–33.

(15) Murdey, R. J.; Salaneck, W. R. Charge Injection Barrier Heights Across Multilayer Organic Thin Films. *Jpn. J. Appl. Phys.* **2005**, *44*, 3751–3756.
(16) Avilov, I.; Geskin, V.; Cornil, J. Quantum-Chemical Characterization of the Origin of Dipole Formation at Molecular Organic/Organic Interfaces. *Adv. Funct. Mater.* **2009**, *19*, 624–633.
(17) Braun, S.; Liu, X.; Salaneck, W. R.; Fahlman, M. Fermi Level Equilibrium at Donor–acceptor Interfaces in Multi-Layered Thin Film Stack of TTF and TCNQ. *Org. Electron.* **2010**, *11*, 212–217.
(18) Mori, T. Organic Charge-Transfer Salts and the Component Molecules in Organic Transistors. *Chem. Lett.* **2011**, *40*, 428–434.
(19) Atalla, V.; Yoon, M.; Caruso, F.; Rinke, P.; Scheffler, M. Hybrid Density Functional Theory Meets Quasiparticle Calculations: A Consistent Electronic Structure Approach. *Phys. Rev. B* **2013**, *88*.
(20) Skulason, H.; Frisbie, C. D. Self-Assembled Monolayers with Charge-Transfer Functional Groups: Immobilization of the Electron Donor TMPD and the Electron Acceptor TCNQ. *Langmuir* **1998**, *14*, 5834–5840.
(21) Santato, C.; Rosei, F. Organic/Metal Interfaces: Seeing Both Sides. *Nat. Chem.* **2010**, *2*, 344–345.
(22) Martínez, J. I.; Abad, E.; Flores, F.; Ortega, J. Simulating the Organic-Molecule/Metal Interface TCNQ/Au(111). *Phys. Status Solidi B* **2011**, n/a-n/a.
(23) Walsh, J.; Davis, R.; Muryn, C.; Thornton, G.; Dhanak, V.; Prince, K. Orientation of Benzene and Pyridine on ZnO (101\= 0). *Phys. Rev. B* **1993**, *48*, 14749.
(24) Hövel, S.; Kolczewski, C.; Wühn, M.; Albers, J.; Weiss, K.; Staemmler, V.; Wöll, C. Pyridine Adsorption on the Polar ZnO(0001) Surface: Zn Termination versus O Termination. *J. Chem. Phys.* **2000**, *112*, 3909.
(25) Hofmann, O. T.; Deinert, J.-C.; Xu, Y.; Rinke, P.; Stähler, J.; Wolf, M.; Scheffler, M. Large Work Function Reduction by Adsorption of a Molecule with a Negative Electron Affinity: Pyridine on ZnO(1010). *J. Chem. Phys.* **2013**, *139*, 174701.
(26) Hofmann, O. T.; Egger, D. A.; Zojer, E. Work-Function Modification beyond Pinning: When Do Molecular Dipoles Count? *Nano Lett.* **2010**, *10*, 4369–4374.
(27) Heyd, J.; Scuseria, G. E.; Ernzerhof, M. Hybrid Functionals Based on a Screened Coulomb Potential. *J. Chem. Phys.* **2003**, *118*, 8207.
(28) Krukau, A. V.; Vydrov, O. A.; Izmaylov, A. F.; Scuseria, G. E. Influence of the Exchange Screening Parameter on the Performance of Screened Hybrid Functionals. *J. Chem. Phys.* **2006**, *125*, 224106.
(29) Oba, F.; Togo, A.; Tanaka, I. Defect Energetics in ZnO: A Hybrid Hartree-Fock Density Functional Study. *Phys. Rev. B* **2008**, *77*.
(30) Moll, N.; Xu, Y.; Hofmann, O. T.; Rinke, P. Stabilization of Semiconductor Surfaces through Bulk Dopants. *New J. Phys.* **2013**, *15*, 83009.
(31) Tkatchenko, A.; Scheffler, M. Accurate Molecular Van Der Waals Interactions from Ground-State Electron Density and Free-Atom Reference Data. *Phys. Rev. Lett.* **2009**, *102*.
(32) Zhang, G.-X.; Tkatchenko, A.; Paier, J.; Appel, H.; Scheffler, M. Van Der Waals Interactions in Ionic and Semiconductor Solids. *Phys. Rev. Lett.* **2011**, *107*, 245501.
(33) Sinai, O.; Hofmann, O. T.; Rinke, P.; Scheffler, M.; Heimel, G.; Kronik, L. Multiscale Approach to the Electronic Structure of Doped Semiconductor Surfaces. *Phys. Rev. B* **2015**, *91*, 75311.
(34) S. Erker et Al., in Preparation.
(35) Scheffler, M. Lattice Relaxations at Substitutional Impurities in Semiconductors. *Phys. BC* **1987**, *146*, 176–186.

(36) Look, D. C.; Reynolds, D. C.; Sizelove, J. R.; Jones, R. L.; Litton, C. W.; Cantwell, G.; Harsch, W. C. Electrical Properties of Bulk ZnO. *Solid State Commun.* **1998**, *105*, 399–401.
(37) Lu, T.; Cotton, T. M.; Birke, R. L.; Lombardi, J. R. Raman and Surface-Enhanced Raman Spectroscopy of the Three Redox Forms of 4,4'-bipyridine. *Langmuir* **1989**, *5*, 406–414.
(38) Yang, H.-H.; McCreery, R. L. Effects of Surface Monolayers on the Electron-Transfer Kinetics and Adsorption of Methyl Viologen and Phenothiazine Derivatives on Glassy Carbon Electrodes. *Anal. Chem.* **1999**, *71*, 4081–4087.
(39) Park, Y. S.; Um, S. Y.; Yoon, K. B. Charge-Transfer Interaction of Methyl Viologen with Zeolite Framework and Dramatic Blue Shift of Methyl Viologen−Arene Charge-Transfer Band upon Increasing the Size of Alkali Metal Cation. *J. Am. Chem. Soc.* **1999**, *121*, 3193–3200.
(40) Hofmann, O. T.; Rangger, G. M.; Zojer, E. Reducing the Metal Work Function beyond Pauli Pushback: A Computational Investigation of Tetrathiafulvalene and Viologen on Coinage Metal Surfaces. *J. Phys. Chem. C* **2008**, *112*, 20357–20365.
(41) Özgür, U.; Alivov, Y. I.; Liu, C.; Teke, A.; Reshchikov, M. A.; Doğan, S.; Avrutin, V.; Cho, S.-J.; Morkoç, H. A Comprehensive Review of ZnO Materials and Devices. *J. Appl. Phys.* **2005**, *98*, 41301.
(42) Duhm, S.; Heimel, G.; Salzmann, I.; Glowatzki, H.; Johnson, R. L.; Vollmer, A.; Rabe, J. P.; Koch, N. Orientation-Dependent Ionization Energies and Interface Dipoles in Ordered Molecular Assemblies. *Nat. Mater.* **2008**, *7*, 326–332.
(43) Hofmann, O. T.; Rinke, P.; Scheffler, M.; Heimel, G. Integer *versus* Fractional Charge Transfer at Metal(/Insulator)/Organic Interfaces: Cu(/NaCl)/TCNE. *ACS Nano* **2015**, *9*, 5391–5404.
(44) Perdew, J. P.; Ruzsinszky, A.; Constantin, L. A.; Sun, J.; Csonka, G. I. Some Fundamental Issues in Ground-State Density Functional Theory: A Guide for the Perplexed. *J. Chem. Theory Comput.* **2009**, *5*, 902–908.
(45) Hofmann, D.; Kümmel, S. Integer Particle Preference during Charge Transfer in Kohn-Sham Theory. *Phys. Rev. B* **2012**, *86*.
(46) Blum, V.; Gehrke, R.; Hanke, F.; Havu, P.; Havu, V.; Ren, X.; Reuter, K.; Scheffler, M. Ab Initio Molecular Simulations with Numeric Atom-Centered Orbitals. *Comput. Phys. Commun.* **2009**, *180*, 2175–2196.
(47) Levchenko, S. V.; Ren, X.; Wieferink, J.; Johanni, R.; Rinke, P.; Blum, V.; Scheffler, M. Hybrid Functionals for Large Periodic Systems in an All-Electron, Numeric Atom-Centered Basis Framework. *Comput. Phys. Commun.* **2015**, *192*, 60–69.
(48) Neugebauer, J.; Scheffler, M. Adsorbate-Substrate and Adsorbate-Adsorbate Interactions of Na and K Adlayers on Al(111). *Phys. Rev. B* **1992**, *46*, 16067–16080.
(49) Janotti, A.; Varley, J. B.; Rinke, P.; Umezawa, N.; Kresse, G.; Van de Walle, C. G. Hybrid Functional Studies of the Oxygen Vacancy in TiO_{2}. *Phys. Rev. B* **2010**, *81*, 85212.
(50) Perdew, J. P.; Burke, K.; Ernzerhof, M. Generalized Gradient Approximation Made Simple. *Phys. Rev. Lett.* **1996**, *77*, 3865–3868.
(51) Janotti, A.; Van de Walle, C. G. Native Point Defects in ZnO. *Phys. Rev. B* **2007**, *76*.
(52) Scheffler, M. Lattice Relaxations at Substitutional Impurities in Semiconductors. *Phys. BC* **1987**, *146*, 176–186.
(53) Richter, N. A.; Sicolo, S.; Levchenko, S. V.; Sauer, J.; Scheffler, M. Concentration of Vacancies at Metal-Oxide Surfaces: Case Study of MgO(100). *Phys. Rev. Lett.* **2013**, *111*, 45502.

Table of contents entry.

Band bending in transparent conductive oxides can significantly impair its transport properties. In the present contribution, we demonstrate how self-assembled monolayers, adsorbed between the inorganic substrate and a strong electron acceptor, can be used to control and tune the band-bending behavior. Utilizing such structures may facilitate the development of organic electronic devices with superior overall performance and a better long-term stability.

Keywords:

Density functional theory, self-assembled monolayers, band bending, charge reservoir electrostatic sheet technique, zinc oxide, TCNQ, hybrid functionals.

Oliver T. Hofmann and Patrick Rinke*

Title: **Band bending engineering at organic/inorganic interfaces using organic self-assembled monolayers**

ToC figure ((Please choose one size: 55 mm broad × 50 mm high **or** 110 mm broad × 20 mm high. Please do not use any other dimensions))